Available online at www.sciencedirect.com
SCIENCE DIRECT®
Journal of Computational Physics 190 (2003) 159–183
JOURNAL OF COMPUTATIONAL PHYSICS
www.elsevier.com/locate/jcp

An upwinding embedded boundary method for Maxwell's equations in media with material interfaces: 2D case

Wei Cai *, Shaozhong Deng

Department of Mathematics, University of North Carolina at Charlotte, Charlotte, NC 28223, USA

Received 15 May 2002; received in revised form 10 February 2003; accepted 12 May 2003

Abstract

We propose a new upwinding embedded boundary method to solve time dependent Maxwell's equations in media with material interfaces. A global second order finite difference method is obtained by combining central difference schemes away from the interfaces and upwinding technique with jump conditions near the interfaces. The proposed finite difference method allows time step based on a uniform mesh independent of the locations and shapes of the interfaces. Moreover, the scheme is simple to implement in multidimensional cases. Numerical tests of wave equations with various types of material interfaces and electromagnetic scattering of 2D cylinders confirm the stability, uniform accuracy and ease of implementation of the method.

AMS: 65M06; 78A45

Keywords: Finite difference time domain method; Cartesian grid methods; Electromagnetic scattering

1. Introduction

Time domain solutions of Maxwell's equations have found applications in engineering problems such as the design of wide band antennas, study of cross talk and signal integrity in VLSI chip designs [1]. In contrast to frequency domain approaches where time harmonic Maxwell's equations are solved for given frequencies [2], the solutions from time domain simulation can produce a wide range of frequency information as well as transient phenomena required in many applications.

The most used time domain algorithm for Maxwell's equations is the simple Yee's finite difference scheme [3], which yields a second order approximation to the fields provided the underlying grids are rectangles and

* Corresponding author. Tel.: +704-687-4581; fax: +704-687-6415.
E-mail address: wcai@uncc.edu (W. Cai).

0021-9991/$ - see front matter
doi:10.1016/S0021-9991(03)00269-9

the conductor or dielectric boundaries are aligning with the mesh coordinates. Thus, the major disadvantage of the Yee's scheme is the limitation of the boundary or material interface geometry. To have second order accuracy, the scheme demands a locally conforming mesh to the boundary. As a result, tiny finite difference cells will limit the time step of the overall scheme. There are some attempts to avoid this limitation on the time step by using extrapolations and the staggered grids of the Yee's scheme for **E** field and **H** field [4].

Recently, discontinuous Galerkin methods have attracted much research to handle the material interfaces in the media. Being higher order versions of traditional finite volume method [5], discontinuous Galerkin methods have been developed initially in 1970s for the study of neutron transport equations [6], and have now been applied to the area of computational fluid dynamics and the solution of Maxwell's equations [7,8]. Discontinuous Galerkin methods inherit the flexibility of the finite element method in allowing unstructured meshes, and at the same time, employ high order polynomials for better accuracy and phase error in modeling wave propagations.

However, to maintain the high order accuracy of discontinuous Galerkin methods, it is important to generate a finite element type of mesh conforming to the interface geometry. The generation of such a mesh consumes a majority of the computational cost and storage requirement. Therefore, in this paper, we propose a new upwinding embedded boundary method which employs a simple Cartesian grid to solve time dependent Maxwell's equations. Cartesian grid based methods have been developed extensively for the shock wave computations [9,10]. The proposed embedded boundary method, like the immersed interface method (IIM) proposed to solve elliptic PDEs with discontinuous coefficients [11], uses a central difference scheme for mesh points away from the interfaces while modifications are made for grid points near the interfaces. The immersed interface method uses a central difference formula at all grid points, therefore, in order to have the difference formula to the correct order of accuracy, jump conditions of the solutions and their derivatives (by using the differential equations) are needed. In [12], the immersed interface method was extended to hyperbolic equations.

In this paper, realizing that information of the solution of the hyperbolic equation is propagated by characteristics and jump conditions across the material interfaces, we believe that it is natural to apply an upwinding strategy to construct difference formulas near the material interfaces. This belief leads to the basic idea of the proposed upwinding embedded boundary method (UEBM), which keeps the simplicity of the Cartesian grid based methods, and provides uniformly accurate and stable numerical solution at a time step allowed on the otherwise uniform mesh, independent of the interface location and geometry.

Various numerical tests presented in this paper show that the proposed upwinding embedded boundary method is simple to code and implement, and produce uniformly second order accurate and stable results. It can be extended with only minor modifications to 3D cases.

The rest of the paper is given as follows: in Section 2, we will demonstrate the idea of the UEBM with a simple 1D scalar model equation. We will show how the solution is passed across the material interface by characteristics and jump conditions, and how the maximum time step allowed on the uniform mesh is achieved independent of the interface location. In Section 3, we extend the method to 1D system by local characteristic decompositions near the interface. In Section 4, we extend the UEBM to 2D Maxwell's equations. In the 2D case, a key technical issue is how to construct one-sided difference formula for an interface with cone property. In Section 5, a series of numerical tests are presented to demonstrate the simplicity, global second order accuracy and stability of the proposed method. Finally, the stability analysis of the proposed method for a 1D model wave equation is included in Appendix A.

2. 1D scalar model equation

In this section, we consider a simple linear wave equation to demonstrate the basic idea of the upwinding embedded boundary method.

Consider a scalar wave equation

$$\frac{\partial u}{\partial t} + a\frac{\partial u}{\partial x} = 0, \quad 0 \leqslant x \leqslant 1, \tag{2.1}$$

where the wave speed a is assumed to be positive and discontinuous at $x_d \in (0,1)$, i.e.,

$$a = \begin{cases} a^- > 0, & x < x_d, \\ a^+ > 0, & x > x_d, \end{cases}$$

and the solution $u(x,t)$ satisfies a jump condition at x_d as follows.

$$r^+ u(x_d^+, \cdot) - r^- u(x_d^-, \cdot) = g. \tag{2.2}$$

For a uniform grid $\{x_i = i\Delta x, 0 \leqslant i \leqslant N, \Delta x = 1/N\}$, we have the numerical solutions u_i^n at grid points (x_i, t^n), $i = 0, 1, \ldots, N$, and also the solutions at both sides of the jump location x_d denoted as u_-^n, u_+^n (see Fig. 1).

We will construct a uniformly second order finite difference method to solve (2.1) based on the Lax–Wendroff approach

$$u^{n+1} \doteq u^n + \Delta t u_t^n + \frac{(\Delta t)^2}{2} u_{tt}^n = u^n - a\Delta t u_x^n + \frac{(a\Delta t)^2}{2} u_{xx}^n, \tag{2.3}$$

where $\Delta t = \mathrm{CFL}(\Delta x/|a|)$, and the spatial derivatives can be approximated by appropriate finite differences such as

$$u_{x,i}^n = u_x^n|_{x=x_i} \sim \sum_{k=-m}^{l} c_k u_{i+k}^n, \tag{2.4}$$

$$u_{xx,i}^n = u_{xx}^n|_{x=x_i} \sim \sum_{k=-m}^{l} d_k u_{i+k}^n, \tag{2.5}$$

where the width of the stencil will be $l + m + 1$. For $l = m$ we have a central difference scheme, and otherwise, a one-sided difference scheme which will be used in place near the domain boundaries and the discontinuity x_d.

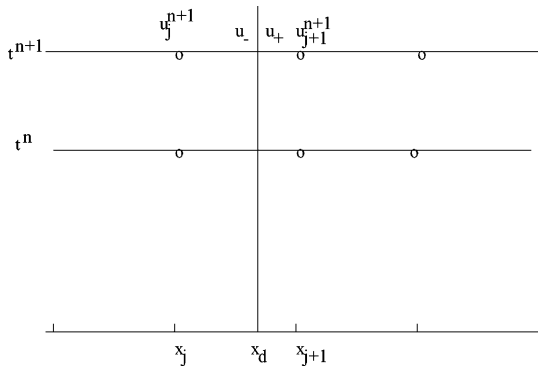

Fig. 1. 1D mesh with discontinuity at x_d.

Let us assume that the solutions u_i^n, $0 \leqslant i \leqslant N$, u_-^n and u_+^n have been obtained for the time step $t = t^n$. We will show how to obtain the solutions at the time step $t = t^{n+1}$. Also, let us assume that

$$x_d \in [x_j, x_{j+1}],$$

and $x_d = x_j + \alpha\Delta x$, $x_{j+1} - x_d = \beta\Delta x$, where $\alpha + \beta = 1$.

2.1. Solutions at the jump x_d

As the solution of (2.1) represents a wave propagating from left to right, we can thus use the PDE (2.1) to obtain u_-^{n+1} at the left side of x_d, namely

$$u_-^{n+1} = u_-^n - a^-\Delta t u_{x,-}^n + \frac{(a^-\Delta t)^2}{2} u_{xx,-}^n, \tag{2.6}$$

where the derivatives $u_{x,-}^n$ and $u_{xx,-}^n$ can be approximated by one-sided difference formulas

$$u_{x,-}^n = u_x^n|_{x=x_d^-} \sim \frac{1}{\Delta x}\left(c_0 u_-^n + \sum_{k=1}^{m} c_k u_{j-k}^n\right), \tag{2.7}$$

$$u_{xx,-}^n = u_{xx}^n|_{x=x_d^-} \sim \frac{1}{(\Delta x)^2}\left(d_0 u_-^n + \sum_{k=1}^{m} d_k u_{j-k}^n\right), \tag{2.8}$$

and the coefficients are selected to have second order accuracy. It should be brought to the attention that in both difference formulas (2.7) and (2.8), the solution u_j^n is not used. Instead, u_-^n is included so that small mesh size and small time step Δt, due to the presence of the jump location x_d, will not occur.

For second order accuracy, we set $m = 2$. Then the coefficients in (2.7) and (2.8) are

$$\begin{aligned} c_0 &= \frac{3+2\alpha}{(1+\alpha)(2+\alpha)}, \quad d_0 = \frac{2}{(1+\alpha)(2+\alpha)}, \\ c_1 &= \frac{-(2+\alpha)^2}{(1+\alpha)(2+\alpha)}, \quad d_1 = \frac{-2(2+\alpha)}{(1+\alpha)(2+\alpha)}, \\ c_2 &= \frac{(1+\alpha)^2}{(1+\alpha)(2+\alpha)}, \quad d_2 = \frac{2(1+\alpha)}{(1+\alpha)(2+\alpha)}. \end{aligned} \tag{2.9}$$

To obtain the solution at the other side of the jump, we can simply use the jump condition (2.2) and have

$$u_+^{n+1} = \frac{1}{r^+}(g + r^- u_-^{n+1}). \tag{2.10}$$

2.2. Solutions u_j^{n+1} and u_{j+1}^{n+1}

Solution u_j^{n+1} can be obtained by an upwinding finite difference (2.4) and (2.5) by setting $l = 0$.

In order to obtain u_{j+1}^{n+1}, we will use the solution u_+^{n+1} just obtained in (2.10), u_+^n, and $u_{j+1+k}^n, k \geqslant 1$. By examining the domain of influence of the hyperbolic equation, we can see that the characteristic originating from the time-space location (x_d, t^n) will pass the location $(x_{j+1}, t^n + \mathrm{CFL}(\beta\Delta x/|a|))$. Therefore, without the knowledge of u_+^{n+1}, we may only be able to time-march the solution at x_{j+1} with a time step $\mathrm{CFL}(\beta\Delta x/|a|)$,

which could be very small if β approaches to zero. Also, we again intentionally do not use u^n_{j+1} to avoid small spatial mesh size. Specifically, we have the following schemes.

Approach I – upwinding.

$$u^{n+1}_{j+1} = u^n_{j+1} - a^+\Delta t u^n_{x,j+1} + \frac{(a^+\Delta t)^2}{2} u^n_{xx,j+1}, \tag{2.11}$$

where

$$u^n_{x,j+1} = u^n_x|_{x=x_{j+1}} \sim \frac{1}{\Delta x}\left(c_0 u^{n+1}_+ + c_1 u^n_+ + \sum_{k=2}^{m} c_k u^n_{j+k}\right), \tag{2.12}$$

$$u^n_{xx,j+1} = u^n_{xx}|_{x=x_{j+1}} \sim \frac{1}{(\Delta x)^2}\left(d_0 u^{n+1}_+ + d_1 u^n_+ + \sum_{k=2}^{m} d_k u^n_{j+k}\right). \tag{2.13}$$

For second order accuracy, we set $m = 2$, and we have

$$\begin{aligned} c_0 &= \frac{1-\beta}{(\gamma+1)(\beta-\gamma)}, \quad d_0 = \frac{-2}{(\gamma+1)(\beta-\gamma)}, \\ c_1 &= \frac{\gamma-1}{(\beta+1)(\beta-\gamma)}, \quad d_1 = \frac{2}{(\beta+1)(\beta-\gamma)}, \\ c_2 &= \frac{\beta+\gamma}{(\beta+1)(\gamma+1)}, \quad d_2 = \frac{2}{(\beta+1)(\gamma+1)}, \end{aligned} \tag{2.14}$$

where $\gamma = \beta + a^+(\Delta t/\Delta x)$.

Approach II – interpolation. Alternatively, we can simply use interpolation from the already computed solutions at the neighboring points at the time step t^{n+1} to approximate u^{n+1}_{j+1}, namely

$$u^{n+1}_{j+1} = e_0 u^{n+1}_+ + \sum_{k=2}^{m} e_k u^{n+1}_{j+k}. \tag{2.15}$$

For second order accuracy, we can set $m = 3$, and we have

$$e_0 = \frac{2}{(\beta+1)(\beta+2)}, \quad e_2 = \frac{2\beta}{\beta+1}, \quad e_3 = \frac{-\beta}{\beta+2}. \tag{2.16}$$

Numerical experiments later will show that both approaches give accurate and stable results. However, the interpolation approach is much simpler to implement, especially in multidimensional cases.

3. 1D systems

Let us consider the linear system of equations

$$\frac{\partial \mathbf{u}}{\partial t} + A\frac{\partial \mathbf{u}}{\partial x} = 0, \tag{3.1}$$

where

$$\mathbf{u}(x,t) = \begin{pmatrix} u_1(x,t) \\ \vdots \\ u_n(x,t) \end{pmatrix}.$$

The matrix A has different formulas across the discontinuity x_d representing a material interface

$$A = \begin{cases} A^-, & x < x_d, \\ A^+, & x > x_d. \end{cases}$$

The matrix A can be diagonalized as follows:

$$A = P\Lambda P^{-1},$$

where

$$\Lambda = \mathrm{diag}(\lambda_1, \ldots, \lambda_p, \ldots, \lambda_n),$$

$$\lambda_1, \ldots, \lambda_p \geqslant 0, \quad \lambda_{p+1}, \ldots, \lambda_n < 0, \tag{3.2}$$

and p is assumed to be the same on both sides of the interface throughout the paper.

Solution $\mathbf{u}(x,t)$ may be discontinuous across the interface x_d and its values on both sides of the interface are related by the following jump condition.

$$R^+\mathbf{u}_+ - R^-\mathbf{u}_- = \mathbf{g}, \tag{3.3}$$

which can be rewritten in terms of the characteristic variable $\mathbf{w} = P^{-1}\mathbf{u}$ as

$$Q^+\mathbf{w}_+ - Q^-\mathbf{w}_- = \mathbf{g}, \tag{3.4}$$

where $Q^+ = R^+P^+$ and $Q^- = R^-P^-$.

The characteristic variables satisfy decoupled scalar wave equations

$$\frac{\partial w_i}{\partial t} + \lambda_i \frac{\partial w_i}{\partial x} = 0, \quad 0 \leqslant i \leqslant n, \tag{3.5}$$

where the λ_i's may have a jump discontinuity at x_d.

3.1. Solutions at the jump x_d

We will apply the same strategy as in Section 2 to the system of equations on the characteristic variable $\mathbf{w}$.

Let

$$\mathbf{w}_\pm = \begin{pmatrix} \mathbf{w}_\pm^1 \\ \mathbf{w}_\pm^2 \end{pmatrix}$$

be the partition of $\mathbf{w}_\pm$ according to the signs of the eigenvalues in (3.2). Similar to the case of single scalar equation, we know that $\mathbf{w}_-^1 = (w_{1,-}, \ldots, w_{p,-})^{\mathrm{T}}$ can be solved by an upwinding scheme for the differential equation (3.5) as in (2.6). And, $\mathbf{w}_+^2 = (w_{p+1,+}, \ldots, w_{n,+})^{\mathrm{T}}$ can also be obtained by an upwinding scheme from (3.5).

Next, we will apply the jump conditions in characteristic variables to obtain the rest components of the characteristic variables on both sides of x_d.

We first partition the matrices Q^+ and Q^- as

$$Q^\pm = \begin{bmatrix} Q_{11}^\pm & Q_{12}^\pm \\ Q_{21}^\pm & Q_{22}^\pm \end{bmatrix}. \tag{3.6}$$

Then from the jump condition (3.4), we can obtain $\begin{pmatrix} \mathbf{w}_+^1 \\ \mathbf{w}_-^2 \end{pmatrix}$ from the following system of equations

$$\begin{bmatrix} Q_{11}^+ & -Q_{12}^- \\ Q_{21}^+ & -Q_{22}^- \end{bmatrix} \begin{pmatrix} \mathbf{w}_+^1 \\ \mathbf{w}_-^2 \end{pmatrix} = \widetilde{\mathbf{g}}, \tag{3.7}$$

where

$$\widetilde{\mathbf{g}} = \mathbf{g} - \begin{bmatrix} -Q_{11}^- & Q_{12}^+ \\ -Q_{21}^- & Q_{22}^+ \end{bmatrix} \begin{pmatrix} \mathbf{w}_-^1 \\ \mathbf{w}_+^2 \end{pmatrix}.$$

The coefficient matrix above is invertible for well-posed hyperbolic systems.

Finally, we have the solution at x_d

$$\mathbf{u}_\pm = P^\pm \mathbf{w}_\pm. \tag{3.8}$$

3.2. Solutions $\boldsymbol{u}_j^{n+1}$ and $\boldsymbol{u}_{j+1}^{n+1}$

We can obtain the solutions at x_j and x_{j+1} in the same way as in the case of one scalar equation by working with the decoupled scalar wave equations (3.5) for the characteristic variables. Again, two approaches can be used, one by solving the partial differential equation with an upwinding algorithm as in (2.11), and one by using interpolation as in (2.15). In both cases, we have to use the solution at the interface x_d at the time step t^{n+1} obtained in (3.8).

4. 2D Maxwell's equations

Let us consider 2D Maxwell's equations for a z-transverse magnetic (TM) wave [13], where the magnetic field $\mathbf{H}$ is transverse to the z-direction and the electric field $\mathbf{E}$ has only one component along the z-direction, i.e.,

$$\mathbf{H} = (H^x(x,y), H^y(x,y), 0)^{\mathrm{T}}, \quad \mathbf{E} = (0, 0, E^z(x,y))^{\mathrm{T}}.$$

In this case, for a bounded region $\Omega = [0,1]^2$ in the x–y plane, the Maxwell's equations are reduced to the following 2D system of equations

$$\frac{\partial \mathbf{u}}{\partial t} + A\frac{\partial \mathbf{u}}{\partial x} + B\frac{\partial \mathbf{u}}{\partial y} = 0, \quad (x,y) \in \Omega = [0,1]^2, \tag{4.1}$$

with

$$\mathbf{u} = \begin{bmatrix} B_x \\ B_y \\ D_z \end{bmatrix},$$

where $\mathbf{B}$ is the magnetic flux density and $\mathbf{D}$ is the electric flux density

$$\mathbf{B} = \mu\mathbf{H},$$

$$\mathbf{D} = \epsilon\mathbf{E}.$$

Here μ is the magnetic permeability and ϵ is the electric permittivity. And

$$A = \begin{bmatrix} 0 & 0 & 0 \\ 0 & 0 & -\frac{1}{\epsilon} \\ 0 & -\frac{1}{\mu} & 0 \end{bmatrix}, \quad B = \begin{bmatrix} 0 & 0 & \frac{1}{\epsilon} \\ 0 & 0 & 0 \\ \frac{1}{\mu} & 0 & 0 \end{bmatrix}.$$

Across a material interface Γ with a normal $\mathbf{n} = (n_x, n_y)^{\mathrm{T}}$ between two dielectric materials Ω^- and $\Omega^+ (\Omega = \Omega^- \cup \Omega^+)$, we have the boundary conditions for the electric and magnetic fields

$$[\mathbf{n} \cdot \epsilon \mathbf{E}] = 0, \quad [\mathbf{n} \cdot \mu \mathbf{H}] = 0,$$

$$[\mathbf{n} \times \mathbf{E}] = 0, \quad [\mathbf{n} \times \mathbf{H}] = 0,$$

which can be written in the form of (3.3) with

$$R^{\pm} = \begin{bmatrix} -\frac{n_y}{\mu_\pm} & \frac{n_x}{\mu_\pm} & 0 \\ n_x & n_y & 0 \\ 0 & 0 & \frac{1}{\epsilon_\pm} \end{bmatrix}.$$

A uniform Cartesian grid $(x_i, y_j) = (i\Delta x, j\Delta y),\ 0 \leqslant i \leqslant N, 0 \leqslant j \leqslant M,\ \Delta x = 1/N,\ \Delta y = 1/M$, will be used to find the solutions $\mathbf{u}_{i,j}^n$ at grid points and $\mathbf{u}_{d,\pm}^n$ at the interface points $\mathbf{x}_{\mathrm{d}} \in \Gamma$ (Fig. 2). $\mathbf{x}_{\mathrm{d}}$ may be selected to the intersection points of the interface Γ and the Cartesian grid coordinate lines.

A grid point (x_i, y_j) will be labelled as a regular grid point if all nine points in the nine point stencil lie on the same side of the interface. Otherwise it is labelled as an irregular grid point. For regular grid points, we can apply the central Lax–Wendroff scheme. For irregular grid points and the interface points $\mathbf{x}_{\mathrm{d}} \in \Gamma$, we will use the method proposed in Sections 2 and 3 by projecting the system (4.1) along the normal direction. Namely, we consider the reformulated linear system

$$\frac{\partial \mathbf{u}}{\partial t} + A_{\mathbf{n}} \frac{\partial \mathbf{u}}{\partial n} + B_\tau \frac{\partial \mathbf{u}}{\partial \tau} = 0, \tag{4.2}$$

where $\tau = (-n_y, n_x)^{\mathrm{T}}$,

$$A_{\mathbf{n}} = (A, B) \cdot \mathbf{n}, \quad B_\tau = (A, B) \cdot \tau, \tag{4.3}$$

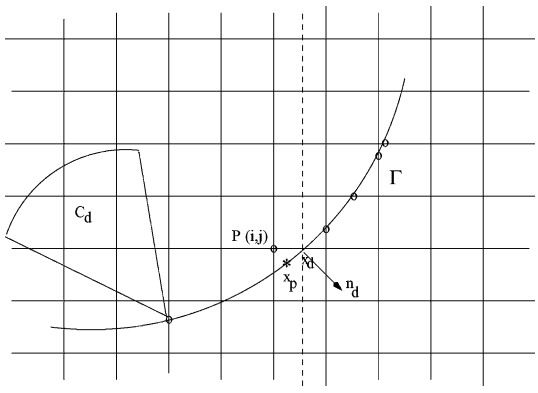

Fig. 2. 2D mesh with material interface Γ.

and

$$\frac{\partial}{\partial n} = \mathbf{n}\cdot\nabla, \frac{\partial}{\partial \tau} = \tau\cdot\nabla.$$

The three eigenvalues of $A_{\mathbf{n}}$ are

$$\lambda_1 = 0, \quad \lambda_2 = c, \quad \lambda_3 = -c, \tag{4.4}$$

where $c = 1/\sqrt{\epsilon\mu}$ is the speed of light in the media. The matrix $P_{\mathbf{n}}^{-1}$ formed by the left row eigenvectors $\mathbf{l}_1$, $\mathbf{l}_2$, $\mathbf{l}_3$ will diagonalize matrix $A_{\mathbf{n}}$

$$A_{\mathbf{n}} = P_{\mathbf{n}} \begin{bmatrix} 0 & & \\ & c & \\ & & -c \end{bmatrix} P_{\mathbf{n}}^{-1},$$

where

$$P_{\mathbf{n}}^{-1} = \begin{bmatrix} \mathbf{l}_1 \\ \mathbf{l}_2 \\ \mathbf{l}_3 \end{bmatrix} = \begin{bmatrix} n_x & n_y & 0 \\ \frac{n_y}{\sqrt{2}} & -\frac{n_x}{\sqrt{2}} & \frac{Z}{\sqrt{2}} \\ -\frac{n_y}{\sqrt{2}} & \frac{n_x}{\sqrt{2}} & \frac{Z}{\sqrt{2}} \end{bmatrix}, \tag{4.5}$$

and $Z = \sqrt{\mu/\epsilon}$ is the intrinsic impedance. Similarly, $P_{\mathbf{n}}$ can be obtained by the right column eigenvectors $\mathbf{r}_1$, $\mathbf{r}_2$, $\mathbf{r}_3$

$$P_{\mathbf{n}} = [\mathbf{r}_1, \mathbf{r}_2, \mathbf{r}_3] = \begin{bmatrix} n_x & \frac{n_y}{\sqrt{2}} & -\frac{n_y}{\sqrt{2}} \\ n_y & -\frac{n_x}{\sqrt{2}} & \frac{n_x}{\sqrt{2}} \\ 0 & \frac{Y}{\sqrt{2}} & \frac{Y}{\sqrt{2}} \end{bmatrix}, \tag{4.6}$$

where $Y = 1/Z$ is the admittance.

The second order finite difference method to solve (4.1) is based on the following time Taylor expansion

$$\mathbf{u}^{n+1} \doteq \mathbf{u}^n + \Delta t \mathbf{u}_t^n + \frac{(\Delta t)^2}{2}\mathbf{u}_{tt}^n = \mathbf{u}^n - \Delta t(A\mathbf{u}_x^n + B\mathbf{u}_y^n) + \frac{(\Delta t)^2}{2}(A^2\mathbf{u}_{xx}^n + (AB+BA)\mathbf{u}_{xy}^n + B^2\mathbf{u}_{yy}^n). \tag{4.7}$$

4.1. Solutions at the interface points $\boldsymbol{x}_d$

Let $\mathbf{n}_{\mathrm{d}} = (n_x, n_y)^{\mathrm{T}}$ be the normal of the interface at $\mathbf{x}_{\mathrm{d}}$, and (x_i, y_j) be the closest irregular grid point in the region Ω^- to $\mathbf{x}_{\mathrm{d}}$ as indicated in Fig. 2. We will discretize the partial derivatives in (4.7) by one-sided difference using only grid values in the region Ω^-.

4.1.1. One-sided difference for almost flat interfaces Γ

When an interface Γ is flat or there are enough grid points along x and y coordinate lines to form regular one-sided difference, the approximation of partial derivatives in (4.7) will be straightforward extension of (2.4) and (2.5).

As $\mathbf{x}_{\mathrm{d}}$ is on one of the Cartesian grid lines, for illustration, let $\mathbf{x}_{\mathrm{d}} = (x_{i+\alpha}, y_j)$, where $x_{i+\alpha} = (i+\alpha)\Delta x$, $0 \leqslant \alpha < 1$, may not be on the grid line, then the following one-sided difference formula can be used to discretize the derivatives in (4.7)

$$\mathbf{u}_x^n|_{\mathbf{x}_{\mathrm{d}}} \sim \sum_{k=0}^{m} c_k \mathbf{u}_{i-k,j}^n, \tag{4.8}$$

$$\mathbf{u}^n_{xx}|_{\mathbf{x}_\mathrm{d}} \sim \sum_{k=0}^{m} d_k \mathbf{u}^n_{i-k,j}, \tag{4.9}$$

while

$$\mathbf{u}^n_{y}|_{\mathbf{x}_\mathrm{d}} \sim \sum_{k=0}^{m} c'_k \mathbf{u}^n_{i+\alpha,j+k}, \tag{4.10}$$

$$\mathbf{u}^n_{yy}|_{\mathbf{x}_\mathrm{d}} \sim \sum_{k=0}^{m} d'_k \mathbf{u}^n_{i+\alpha,j+k}, \tag{4.11}$$

where the solution $\mathbf{u}^n_{i+\alpha,j+k}$ at the location $(x_{i+\alpha},\ y_{j+k})$ can be approximated from values at the nearby grid points, in most cases when possible, by a simple average. The mixed derivative $\mathbf{u}^n_{xy}$ will be handled by two consecutive one-sided difference approximations of x- and y-derivatives.

4.1.2. One-sided difference for interfaces Γ with cone property

For most curved interfaces, the simple one-sided difference may not be applicable as there may not be enough grid points along either of the coordinate lines. For those cases, we propose to use the following least square method, using available grid solutions near the interface points or irregular points, to define the approximation to the partial derivatives. Data fitting by least square has been successfully used in the superconvergence recovery of finite element methods [14]. In order to apply the least square approach, we will limit the interfaces to curves with the so-called cone property. Namely, for each $x_\mathrm{d} \in \Gamma$, there is a cone with its vertex at $\mathbf{x}_\mathrm{d}$ (see Fig. 2)

$$C_\mathrm{d}(r,\theta_1,\theta_2) = \{\mathbf{x} = \mathbf{x}_\mathrm{d} + t(\cos\theta, \sin\theta), \quad 0 \leqslant t \leqslant r, \quad \theta_1 \leqslant \theta \leqslant \theta_2\}, \tag{4.12}$$

such that

$$C_\mathrm{d}(r,\theta_1,\theta_2) \subset \Omega^-, \quad \text{or} \quad \Omega^+. \tag{4.13}$$

We require that (4.12) and (4.13) hold for both Ω^- and Ω^+.

If there are m grid points $\{\mathbf{x}_l = (x_l, y_l), 1 \leqslant l \leqslant m\} \subset C_\mathrm{d}(r,\theta_1,\theta_2)$, we will be able to fit a kth order polynomial $p_k(x,y) \in P_k = \mathrm{span}\{x^i y^j, 0 \leqslant i+j \leqslant k\}$ (assuming that $m > (k+1)(k+2)/2$, in most cases, we only need to have $k = 2$) to each component u_l, $1 \leqslant l \leqslant n$, of the solution vector $\mathbf{u}$ by

$$p_k(x,y) = P^\mathrm{T}\mathbf{a},$$

where $P^\mathrm{T} = (1, \bar{x}, \bar{y}, \bar{x}^2, \ldots, \bar{x}^k, \bar{x}^{k-1}\bar{y}, \ldots, \bar{y}^k)$, $\bar{x} = x - x_\mathrm{d}$, $\bar{y} = y - y_\mathrm{d}$. And the coefficient vector $\mathbf{a}$ can be obtained by a least square procedure which is solved with the following normal equation

$$C^\mathrm{T} C\mathbf{a} = C^\mathrm{T}\mathbf{b},$$

where $\mathbf{b} = (u_l(\mathbf{x}_1), u_l(\mathbf{x}_2), \ldots, u_l(\mathbf{x}_m))^\mathrm{T}$, and

$$C = \begin{bmatrix} 1 & \bar{x}_1 & \bar{y}_1 & \cdots & \bar{y}_1^k \\ 1 & \bar{x}_2 & \bar{y}_2 & \cdots & \bar{y}_2^k \\ 1 & \bar{x}_3 & \bar{y}_3 & \cdots & \bar{y}_3^k \\ \vdots & \vdots & \vdots & \cdots & \vdots \\ 1 & \bar{x}_m & \bar{y}_m & \cdots & \bar{y}_m^k \end{bmatrix}.$$

Then, the derivatives of $u_l(\mathbf{x})$ can be approximated by

$$\nabla^s u_l(\mathbf{x}) = \nabla^s p_k(\mathbf{x}), \quad s = 1, 2. \tag{4.14}$$

Now, with (4.7)–(4.11) and (4.14), we can obtain the solution $\mathbf{u}_{d,-}^{n+1}$. However, we will only use the characteristic components which are outflow components along the normal direction $\mathbf{n}_\mathrm{d}$. We project the solution $\mathbf{u}$ along the eigen-direction of $A_\mathbf{n}$ in (4.3),

$$\mathbf{w}_- = \begin{pmatrix} w_{1,-} \\ w_{2,-} \\ w_{3,-} \end{pmatrix} = (P_\mathbf{n}^-)^{-1}\mathbf{u}_{d,-}^{n+1},$$

and according to the signs of the eigenvalues in (4.4), we decompose $\mathbf{w}_-$ as

$$\mathbf{w}_- = \begin{pmatrix} \mathbf{w}_-^1 \\ \mathbf{w}_-^2 \end{pmatrix}, \quad \mathbf{w}_-^1 = \begin{pmatrix} w_{1,-} \\ w_{2,-} \end{pmatrix}, \quad \mathbf{w}_-^2 = (w_{3,-}),$$

and then based on the upwinding principle, we retain the value of $\mathbf{w}_-^1$ at t^{n+1}.

Similarly, we can apply the same procedure in the region Ω^+ to get the value for $\mathbf{w}_+^2$ based on the characteristic projection using $\mathbf{w}_+ = (P_\mathbf{n}^+)^{-1}\mathbf{u}_{d,+}^{n+1}$.

The rest of characteristic components in $\mathbf{w}_-$ and $\mathbf{w}_+$ can be solved similarly as in (3.7).

4.2. Solutions at the irregular grid points *P*

Let $\mathbf{P} = (x_i, y_j)$ be an irregular grid point on the Cartesian grid (Fig. 2), $\mathbf{x}_p$ be the projection of $\mathbf{P}$ onto the interface Γ in terms of the shortest distance, and $\mathbf{n}_p = (n_x, n_y)^\mathrm{T}$. We will apply the method in Section 3 based on the characteristic decomposition of matrix $A_\mathbf{n} = (A, B) \cdot \mathbf{n}_p$. Again, one-sided difference formulas in (4.8)–(4.11) and (4.14) will be used to approximate the x- and y-derivatives (thus the normal derivative) and the details are omitted here.

5. Numerical results

In this section, several PDEs with available exact solutions are approximated. As our focus is on the capability of the proposed method to handle various types of material interfaces, we will provide the boundary values obtained by the exact solutions. In practical simulations when boundary values are not available, absorbing boundary conditions such as PML boundary condition [15] or Lorentz material model absorber layers [16,17] should be used.

5.1. Linear 1D wave system

In this test, we consider the 1D system (3.1) with

$$A^- = \begin{bmatrix} 0 & 1 \\ 1 & 0 \end{bmatrix}, \quad A^+ = \begin{bmatrix} 0 & 3 \\ 3 & 0 \end{bmatrix}.$$

The exact solution to this system is

In $0 \leqslant x < x_\mathrm{d}$:

$$u_1(x,t) = \tfrac{1}{2}(\sin(k(x+t)) + \sin(k(x-t))),$$

$$u_2(x,t) = -\tfrac{1}{2}(\sin(k(x+t)) - \sin(k(x-t))).$$

In $x_d < x \leqslant 1$:

$$u_1(x,t) = \tfrac{1}{2}(\sin(k(x+3t)) + \sin(k(x-3t))),$$

$$u_2(x,t) = -\tfrac{1}{2}(\sin(k(x+3t)) - \sin(k(x-3t))).$$

The jump condition (3.3) is obtained by the values given by the exact solution at x_d. We set $k = 8\pi$ in our tests. The time step is taken as

$$\Delta t = \mathrm{CFL}\frac{\Delta x}{|\lambda_{\max}|},$$

where $|\lambda_{\max}| = \max_{A^-,A^+}\{|\lambda_{A^-}|, |\lambda_{A^+}|\}$. In our tests, CFL = 0.8.

We will test three cases, $x_d = 0.5 + \Delta x/10^8$, $x_d = 0.5 + \Delta x/2$ and $x_d = 0.5 - \Delta x/10^8$. The numerical results demonstrate the stability of the UEBM with the same time step independent of the interface locations. Tables 1 and 2 show the results of grid refinement analysis for the upwinding approach (2.11) and the interpolation approach (2.15), respectively. The results confirm the global second order accuracy of both approaches. However, as Approach II is simpler to implement in 2D and 3D situations, we will use it for the numerical tests in all 2D cases later. Fig. 3 shows the computed and the exact solutions at the time $t = \pi$ with $x_d = 0.5 + \Delta x/10^8$ and $N = 200$ using the upwinding approach.

To compare the UEBM with the immersed interface method (IIM) for hyperbolic equations [12], we apply the IIM to solve the same 1D wave system. Table 3 shows the results of grid refinement analysis. It can be observed that both methods are second order accurate, and they seem to have consistent accuracy because both use the second order Lax–Wendroff scheme for regular Cartesian grid points.

Both methods can capture jump conditions across material interfaces using Cartesian grid, but the UEBM needs to track the solutions at the interfaces as well. The UEBM also needs local characteristic decompositions near the interfaces. On the other hand, in the IIM method, in order to have the difference

Table 1
The grid refinement analysis for 1D wave system – upwinding approach

N	$x_d = 0.5 + \Delta x/10^8$		$x_d = 0.5 + \Delta x/2$		$x_d = 0.5 - \Delta x/10^8$	
	$\|E_N\|_\infty$	Order	$\|E_N\|_\infty$	Order	$\|E_N\|_\infty$	Order
100	1.018×10^{-1}		8.994×10^{-2}		8.492×10^{-2}	
200	2.522×10^{-2}	2.0130	2.270×10^{-2}	1.9863	2.182×10^{-2}	1.9604
400	6.436×10^{-3}	1.9700	5.706×10^{-3}	1.9921	5.580×10^{-3}	1.9675
800	1.638×10^{-3}	1.9739	1.428×10^{-3}	1.9982	1.402×10^{-3}	1.9932
1600	4.117×10^{-4}	1.9923	3.573×10^{-4}	1.9988	3.521×10^{-4}	1.9934

Table 2
The grid refinement analysis for 1D wave system – interpolation approach

N	$x_d = 0.5 + \Delta x/10^8$		$x_d = 0.5 + \Delta x/2$		$x_d = 0.5 - \Delta x/10^8$	
	$\|E_N\|_\infty$	Order	$\|E_N\|_\infty$	Order	$\|E_N\|_\infty$	Order
100	9.040×10^{-2}		8.566×10^{-2}		9.551×10^{-2}	
200	2.806×10^{-2}	1.6881	2.953×10^{-2}	1.5363	3.013×10^{-2}	1.6642
400	6.408×10^{-3}	2.1303	6.635×10^{-3}	2.1542	6.643×10^{-3}	2.1816
800	1.548×10^{-3}	2.0495	1.577×10^{-3}	2.0732	1.575×10^{-3}	2.0766
1600	3.797×10^{-4}	2.0275	3.839×10^{-4}	2.0384	3.770×10^{-4}	2.0627

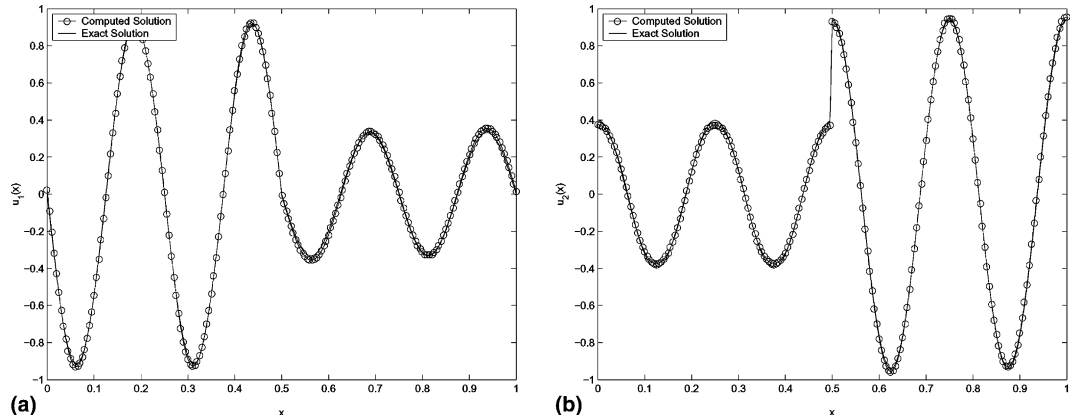

Fig. 3. The computed and the exact solutions for 1D wave system using the upwinding approach ($x_d = 0.5 + \Delta x/10^8, N = 200$): (a) $u_1(x,\pi)$; (b) $u_2(x,\pi)$.

Table 3
The grid refinement analysis for 1D wave system – immersed interface method

N	$x_d = 0.5 + \Delta x/10^8$		$x_d = 0.5 + \Delta x/2$		$x_d = 0.5 - \Delta x/10^8$	
	$\|E_N\|_\infty$	Order	$\|E_N\|_\infty$	Order	$\|E_N\|_\infty$	Order
100	8.376×10^{-2}		8.375×10^{-2}		8.367×10^{-2}	
200	2.108×10^{-2}	1.9904	2.108×10^{-2}	1.9902	2.108×10^{-2}	1.9888
400	5.279×10^{-3}	1.9975	5.279×10^{-3}	1.9975	5.279×10^{-3}	1.9984
800	1.320×10^{-3}	1.9997	1.320×10^{-3}	1.9997	1.320×10^{-3}	1.9997
1600	3.304×10^{-4}	1.9983	3.304×10^{-4}	1.9983	3.304×10^{-4}	1.9983

formula to the correct order of accuracy, jump conditions of not only the solutions but also their derivatives are needed. Because the derived jump conditions at the interface depend on the differential equations themselves, the derivation of the jump conditions may be very complicated.

5.2. Comparison between the Yee's scheme and the UEBM: plane wave normally incident on a planar boundary

To compare the behaviors of the standard Yee's scheme and the UEBM, we consider the following 1D Maxwell's equations

$$\epsilon \frac{\partial E}{\partial t} = \frac{\partial H}{\partial z},$$

$$\mu \frac{\partial H}{\partial t} = \frac{\partial E}{\partial z},$$

where $E(z,t)$ and $H(z,t)$ signify the mutually perpendicular tangential electric and magnetic field components (E_y, H_x).

We first solve the above 1D Maxwell's equations in a homogeneous medium with $\epsilon = 2$ and $\mu = 2$. Table 4 shows the results of grid refinement analysis for both the Yee's scheme and the UEBM. It is clear that in a homogeneous medium, both methods are second order accurate, and there are no essential differences in accuracy.

Table 4
Comparison between the Yee's scheme and the UEBM for 1D Maxwell's equations – homogeneous medium ($\epsilon = \mu = 2$)

N	Yee's scheme		UEBM	
	$\|E_N\|_\infty$	Order	$\|E_N\|_\infty$	Order
100	1.711×10^{-2}		1.621×10^{-2}	
200	4.279×10^{-3}	1.9995	3.982×10^{-3}	2.0253
400	1.070×10^{-3}	1.9997	9.884×10^{-4}	2.0103
800	2.675×10^{-4}	2.0000	2.463×10^{-4}	2.0047
1600	6.688×10^{-5}	1.9999	6.149×10^{-5}	2.0020

We then take the simple example of a plane wave normally incident on a planar boundary ($z = 0$) [18]. On the left of the boundary ($-0.5 \leqslant z \leqslant 0$), the medium is vacuum ($\epsilon_1 = \mu_1 = 1$), but the medium on the right ($0 \leqslant z \leqslant 0.5$) is a dielectric with $\epsilon_2 = 2$ and $\mu_2 = 2$. When the incident wave encounters the interface, a reflective wave and a transmitted wave will be generated. To solve the wave propagation problem, the above 1D Maxwell's equations are used. In our test, the incident plane wave takes the form

$$E_{\text{inc}} = \mathrm{e}^{\mathrm{i}(\omega t + k_1 z)}, \quad H_{\text{inc}} = \frac{1}{Z_1}\mathrm{e}^{\mathrm{i}(\omega t + k_1 z)}.$$

Then the problem has an exact solution given as follows

$$E(z,t) = \begin{cases} \mathrm{e}^{\mathrm{i}(\omega t + k_1 z)} + \frac{Z_2 - Z_1}{Z_2 + Z_1}\mathrm{e}^{\mathrm{i}(\omega t - k_1 z)}, & z < 0, \\ \frac{2Z_2}{Z_2 + Z_1}\mathrm{e}^{\mathrm{i}(\omega t + k_2 z)}, & z > 0, \end{cases}$$

$$H(z,t) = \begin{cases} \frac{1}{Z_1}\mathrm{e}^{\mathrm{i}(\omega t + k_1 z)} - \frac{Z_2 - Z_1}{Z_1(Z_2 + Z_1)}\mathrm{e}^{\mathrm{i}(\omega t - k_1 z)}, & z < 0, \\ \frac{2}{Z_2 + Z_1}\mathrm{e}^{\mathrm{i}(\omega t + k_2 z)}, & z > 0, \end{cases}$$

where $k_1 = \omega\sqrt{\epsilon_1\mu_1}$ and $k_2 = \omega\sqrt{\epsilon_2\mu_2}$ are the propagation constants, and $Z_1 = \sqrt{\mu_1/\epsilon_1}$ and $Z_2 = \sqrt{\mu_2/\epsilon_2}$ are the impedances of the media.

Table 5 shows the results of grid refinement analysis for both the Yee's scheme and the UEBM. The results clearly show that the global accuracy of the UEBM remains second order, but that of the Yee's scheme is reduced to first order because it cannot model the material interface correctly. And for this example, for a realistic accuracy around 1%, the UEBM ends up superior.

Table 5
Comparison between the Yee's scheme and the UEBM for 1D Maxwell's equations – inhomogeneous media ($\epsilon_1 = \mu_1 = 1$ and $\epsilon_2 = \mu_2 = 2$)

N	Yee's scheme		UEBM	
	$\|E_N\|_\infty$	Order	$\|E_N\|_\infty$	Order
100	5.759×10^{-2}		1.417×10^{-2}	
200	2.214×10^{-2}	1.3792	3.558×10^{-3}	1.9937
400	9.445×10^{-3}	1.2290	8.922×10^{-4}	1.9956
800	4.327×10^{-3}	1.1262	2.234×10^{-4}	1.9977
1600	2.064×10^{-3}	1.0679	5.591×10^{-5}	1.9985

5.3. Linear 2D wave system

In this test, we will verify the second order accuracy of the UEBM for the linear 2D wave equations for various types of material interfaces. We shall consider a 2D wave system (4.1) for two unknowns with the following coefficient matrices A and B.

In Ω^-:

$$A^- = \begin{bmatrix} 2 & -1 \\ -1 & 2 \end{bmatrix}, \quad B^- = \begin{bmatrix} 2 & 0 \\ 0 & 1 \end{bmatrix}.$$

In Ω^+ :

$$A^+ = \begin{bmatrix} 4 & -2 \\ -2 & 4 \end{bmatrix}, \quad B^+ = \begin{bmatrix} 4 & 0 \\ 0 & 2 \end{bmatrix}.$$

The exact solution to this system is

In Ω^- :

$$u_1(x,y,t) = \sin(k(x-t)) + \sin(k(y-2t)),$$

$$u_2(x,y,t) = \sin(k(x-t)) + \sin(k(y-t)).$$

In Ω^+ :

$$u_1(x,y,t) = \sin(k(x-2t)) + \cos(k(y-4t)),$$

$$u_2(x,y,t) = \sin(k(x-2t)) + \cos(k(y-2t)).$$

The jump condition (3.3) is obtained by the values given by the exact solution at a given interface Γ. In our test $k = 4\pi$ unless otherwise specified, and $\Delta x = \Delta y = h$. The time step is chosen as

$$\Delta t = \mathrm{CFL}\frac{h}{2\sqrt{2}|\lambda_{\max}|},$$

where $|\lambda_{\max}| = \max_{A^\pm, B^\pm}\{|\lambda_{A^-}|, |\lambda_{A^+}|, |\lambda_{B^-}|, |\lambda_{B^+}|\}$. In our test, we set $\mathrm{CFL} = 0.8$, independent of the locations and shapes of the interfaces.

Case 1. Γ is a line with 45° inclination with respect to the x-axis. In Table 6, we list the error and convergence rate for three situations with different distances h_Γ between the interface Γ and the mesh points. $h_\Gamma = 10^{-8}\Delta x$ means that Γ is close to the grid points from above. $h_\Gamma = \Delta x/1.000000001$ means that Γ is close to the grid points from below. Again, uniformly second order convergence is observed in all three situations. Fig. 4 shows the contour of the computed solution of $u_1(x,y,t=1)$ for the situation $h_\Gamma = \Delta x/1.000000001$, and Fig. 5 shows slices of the computed and the exact solutions of $u_1(x,y,t=1)$ at $y = 0.5$.

Case 2. In this case, we let the inclination of the interface Γ with respect to the x-axis to be 1° or 89°, which corresponds to the situation where the interface is almost aligned with a coordinate line. In Table 7, again, uniformly second order convergence is observed.

Case 3. We consider the interface Γ to be the circle $x^2 + y^2 = r^2$ with $r = 0.6$, and the solution domain to be $\Omega = [-1,1]^2$. We set $k = 2\pi$ in this case. Fig. 6 shows the contour of the computed solution of $u_1(x,y,t=1.5)$, and Fig. 7 shows slices of the computed and the exact solutions of $u_1(x,y,t=1.5)$ at $y = 0$. Table 8 shows the second order convergence of the maximum error for four different meshes.

Table 6
The grid refinement analysis for 2D wave system – line with 45° inclination

$N \times M$	$h_\Gamma = \Delta x/10^8$		$h_\Gamma = \Delta x/2$		$h_\Gamma = \Delta x/1.000000001$	
	$\|E_N\|_\infty$	Order	$\|E_N\|_\infty$	Order	$\|E_N\|_\infty$	Order
50×50	3.519×10^{-1}		3.396×10^{-1}		3.407×10^{-1}	
100×100	8.319×10^{-2}	2.0807	7.879×10^{-2}	2.1078	7.703×10^{-2}	2.1450
200×200	2.032×10^{-2}	2.0331	2.097×10^{-2}	1.9097	2.112×10^{-2}	1.8664
400×400	5.274×10^{-3}	1.9464	5.388×10^{-3}	1.9605	5.439×10^{-3}	1.9576

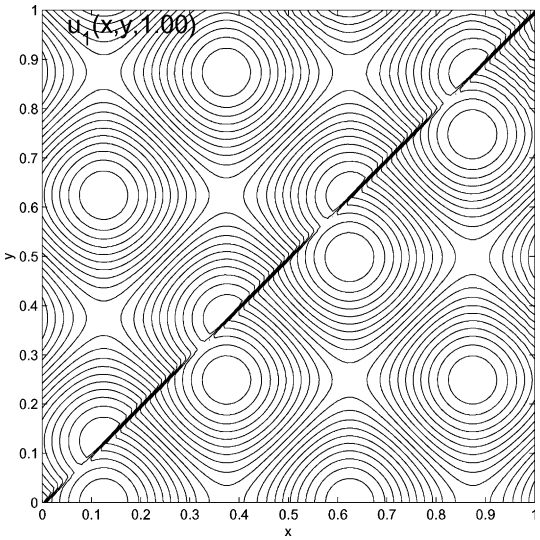

Fig. 4. Contour of the computed solution of $u_1(x, y, t = 1)$ for 2D wave system – line with 45° inclination ($h_\Gamma = \Delta x/1.000000001$ and 100×100 mesh).

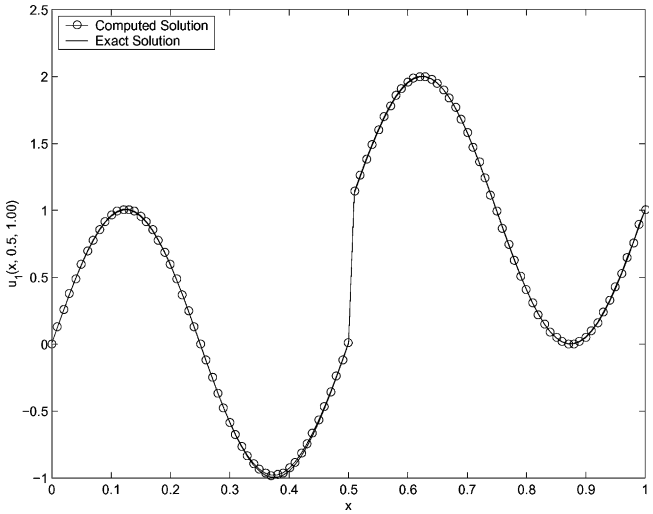

Fig. 5. Slices of the computed and the exact solutions of $u_1(x, y, t = 1)$ at $y = 0.5$ for 2D wave system – line with 45° inclination ($h_\Gamma = \Delta x/1.000000001$ and 100×100 mesh).

Table 7
The grid refinement analysis for 2D wave system – line with 1° or 89° inclination

$N \times M$	Inclination = 1°		Inclination = 89°	
	$\|E_N\|_\infty$	Order	$\|E_N\|_\infty$	Order
50×50	3.231×10^{-1}		2.488×10^{-1}	
100×100	8.939×10^{-2}	1.8537	6.366×10^{-2}	1.9662
200×200	2.299×10^{-2}	1.9593	1.571×10^{-2}	2.0187
400×400	5.911×10^{-3}	1.9594	3.942×10^{-3}	1.9949

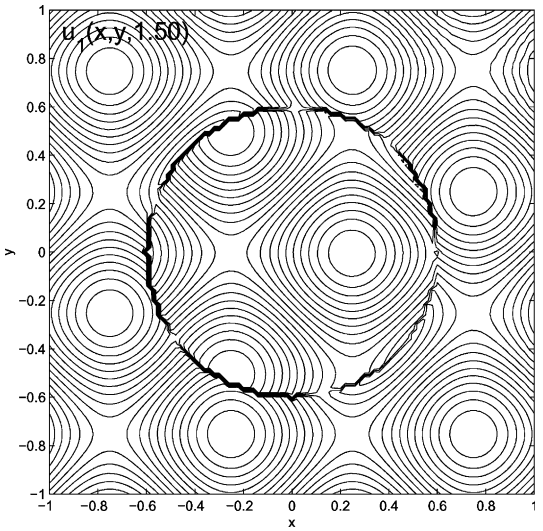

Fig. 6. Contour of the computed solution of $u_1(x, y, t = 1.5)$ for 2D wave system – circle with radius of 0.6 (100×100 mesh).

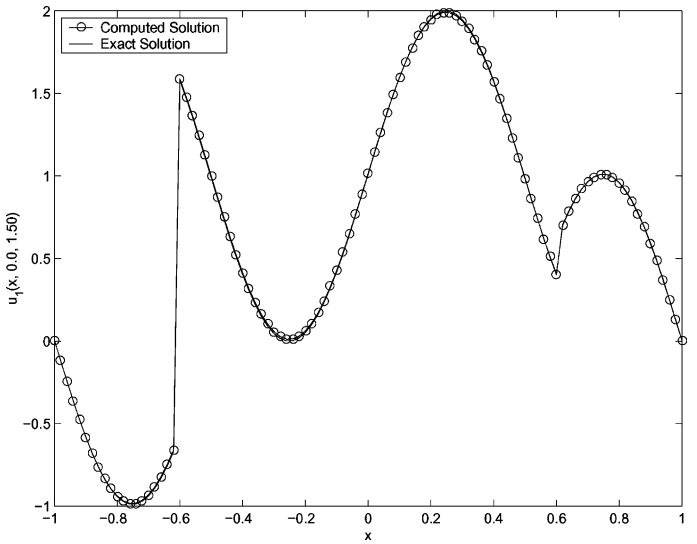

Fig. 7. Slices of the computed and the exact solutions of $u_1(x, y, t = 1.5)$ at $y = 0$ for 2D wave system – circle with radius of 0.6 (100×100 mesh).

Table 8
The grid refinement analysis for 2D wave system – circle with radius of 0.6

$N \times M$	$\|E_N\|_\infty$	Order
50×50	3.594×10^{-1}	
100×100	7.458×10^{-2}	2.2688
200×200	1.328×10^{-2}	2.4891
400×400	3.120×10^{-3}	2.0901

5.4. Scattering of a dielectric cylinder

In this test, we shall focus the attention on solving the following 2D TM form Maxwell's equations for (H^x, H^y, E^z)

$$\frac{\partial \mu H^x}{\partial t} = -\frac{\partial E^z}{\partial y},$$

$$\frac{\partial \mu H^y}{\partial t} = \frac{\partial E^z}{\partial x},$$

$$\frac{\partial \epsilon E^z}{\partial t} = \frac{\partial H^y}{\partial x} - \frac{\partial H^x}{\partial y}.$$

The field components, (H_k^x, H_k^y, E_k^z), are subject to boundary conditions between two regions, with material parameters ϵ_k and μ_k, for $k = 1, 2$, as

$$\mathbf{n} \times \mathbf{H}_1 = \mathbf{n} \times \mathbf{H}_2,$$

$$\mathbf{n} \cdot \mu_1 \mathbf{H}_1 = \mathbf{n} \cdot \mu_2 \mathbf{H}_2,$$

$$E_1^z = E_2^z.$$

Here, $\mathbf{H}_k = (H_k^x, H_k^y, 0)^{\mathrm{T}}$, and $\mathbf{n} = (n_x, n_y, 0)^{\mathrm{T}}$ represents a unit normal to the material interface.

We shall consider a typical electromagnetic scattering problem, i.e., scattering by a dielectric cylinder in free space with a TM wave excitation. An illustration is shown in Fig. 8. The cylinder is assumed to have a radius of r_0.

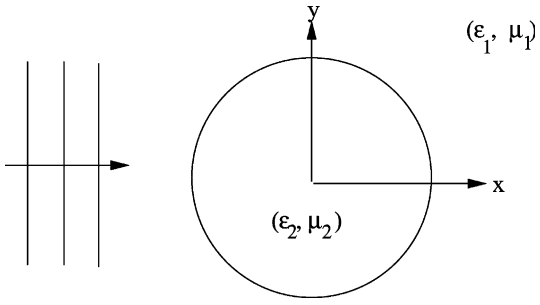

Fig. 8. Scattering of a 2D dielectric cylinder.

If we assume that the cylinder is illuminated by a time-harmonic incident plane unit wavelength wave of the form

$$E^z_{\text{inc}} = \mathrm{e}^{-\mathrm{i}(k_1 x-\omega t)}, \quad H^y_{\text{inc}} = -\mathrm{e}^{-\mathrm{i}(k_1 x-\omega t)},$$

where the propagation constant for homogeneous, isotropic free-space medium is $k_1 = \omega\sqrt{\mu_1\epsilon_1}$, then the problem has an exact solution [19] given as follows

$$E^z(x,y,t) = E^z(r,\theta,t) = \mathrm{e}^{\mathrm{i}\omega t}\begin{cases} \sum_{n=-\infty}^{\infty} C_n^{\text{tot}} J_n(k_2 r)\mathrm{e}^{\mathrm{i}n\theta}, & r \leqslant r_0, \\ \sum_{n=-\infty}^{\infty} (\mathrm{i}^{-n} J_n(k_1 r) + C_n^{\text{scat}} H_n^{(2)}(k_1 r))\mathrm{e}^{\mathrm{i}n\theta}, & r > r_0, \end{cases}$$

where $(r,\theta) = (\sqrt{x^2+y^2}, \arctan(y/x))$ represent the usual polar coordinates, J_n and $H_n^{(2)}$ represent the nth order Bessel function of the first kind and the Hankel function of the second kind, respectively, and $k_2 = \omega\sqrt{\mu_2\epsilon_2}$ is the propagation constant for homogeneous, lossless dielectric medium.

The expansion coefficients for the total field interior to the cylinder are given as

$$C_n^{\text{tot}} = \mathrm{i}^{-n}\frac{(k_1/\mu_1)J_n'(k_1 r_0)H_n^{(2)}(k_1 r_0) - (k_1/\mu_1)H_n^{(2)'}(k_1 r_0)J_n(k_1 r_0)}{(k_2/\mu_2)J_n'(k_2 r_0)H_n^{(2)}(k_1 r_0) - (k_1/\mu_1)H_n^{(2)'}(k_1 r_0)J_n(k_2 r_0)},$$

and

$$C_n^{\text{scat}} = \mathrm{i}^{-n}\frac{(k_1/\mu_1)J_n'(k_1 r_0)J_n(k_2 r_0) - (k_2/\mu_2)J_n'(k_2 r_0)J_n(k_1 r_0)}{(k_2/\mu_2)J_n'(k_2 r_0)H_n^{(2)}(k_1 r_0) - (k_1/\mu_1)H_n^{(2)'}(k_1 r_0)J_n(k_2 r_0)}.$$

Use Maxwell's equations, one can obtain the solutions for the magnetic field components. Actually the angular component of the total magnetic field is given as

$$H^\theta(r,\theta,t) = -\mathrm{e}^{\mathrm{i}\omega t}\begin{cases} \frac{-\mathrm{i}k_2}{\omega\mu_2}\sum_{n=-\infty}^{\infty} C_n^{\text{tot}} J_n'(k_2 r)\mathrm{e}^{\mathrm{i}n\theta}, & r \leqslant r_0, \\ \frac{-\mathrm{i}k_1}{\omega\mu_1}\sum_{n=-\infty}^{\infty} (\mathrm{i}^{-n} J_n'(k_1 r) + C_n^{\text{scat}} H_n^{(2)'}(k_1 r))\mathrm{e}^{\mathrm{i}n\theta}, & r > r_0, \end{cases}$$

and the radial component is given by

$$H^r(r,\theta,t) = -\mathrm{e}^{\mathrm{i}\omega t}\begin{cases} \frac{\mathrm{i}}{\omega\mu_2 r}\sum_{n=-\infty}^{\infty} \mathrm{i}n C_n^{\text{tot}} J_n(k_2 r)\mathrm{e}^{\mathrm{i}n\theta}, & r \leqslant r_0, \\ \frac{\mathrm{i}}{\omega\mu_1 r}\sum_{n=-\infty}^{\infty} \mathrm{i}n(\mathrm{i}^{-n} J_n(k_1 r) + C_n^{\text{scat}} H_n^{(2)}(k_1 r))\mathrm{e}^{\mathrm{i}n\theta}, & r > r_0. \end{cases}$$

We consider a situation in which $\mu_1 = \epsilon_1 = 1$, i.e., the material exterior to the cylinder is assumed to be vacuum. We consider two types of cylinders. In the first case, we set $\mu_2 = 1$, i.e., the material is non-magnetics. In this special case, all three field components are continuous across the material interface. The derivative of E^z is also continuous across the interface, but derivatives of H^x and H^y are discontinuous. In the second case, we set $\mu_2 = 2$. In this case, E^z is continuous across the interface, but H^x, H^y and derivatives of H^x, H^y, and E^z are all discontinuous.

In the numerical tests, we set the permittivity of the cylinder $\epsilon_2 = 2.25$, the radius of the cylinder $r_0 = 0.6$ and the angular frequency $\omega = 2\pi$. The computational domain is set as $[-1,1]^2$, and in all computations, we let $\Delta x = \Delta y = h$. The time step used in the computations is

$$\Delta t = \text{CFL}\frac{h}{2\sqrt{2}\lambda_{\max}},$$

where $\lambda_{\max} = \max\{c_1, c_2\}$ and $c_k = 1/\sqrt{\epsilon_k\mu_k}$, for $k = 1, 2$. $\lambda_{\max}$ equals to 1 and CFL is set as 0.5 in our test.

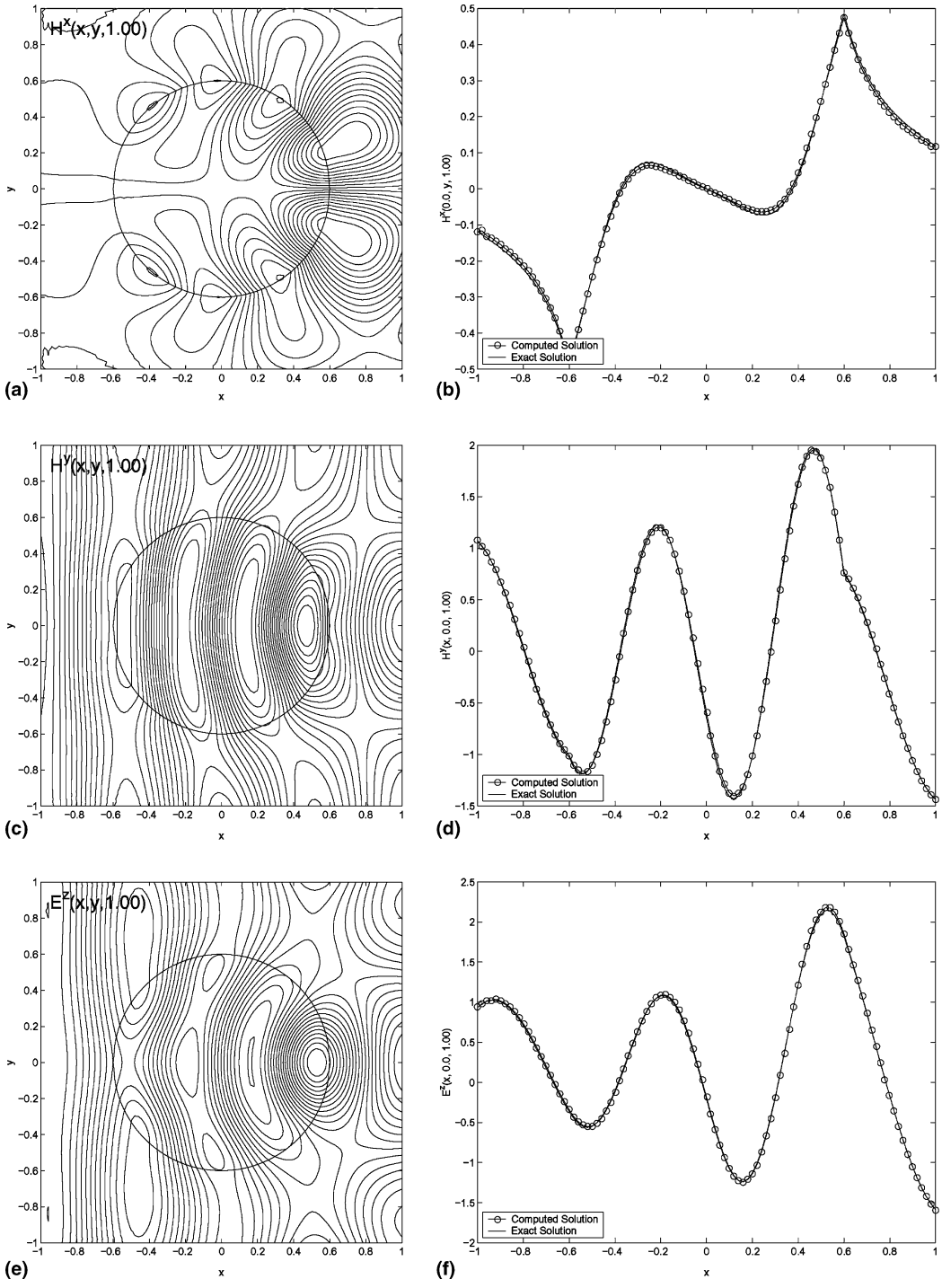

Fig. 9. Scattering of a 2D dielectric cylinder with material parameters $\mu_1 = \mu_2 = \epsilon_1 = 1$ and $\epsilon_2 = 2.25$. On the left are contours of the computed solutions, and on the right are slices of the computed and the exact solutions. (a) $H^x(x, y, t = 1.0)$; (b) $H^x(0, y, t = 1.0)$; (c) $H^y(x, y, t = 1.0)$; (d) $H^y(x, 0, t = 1.0)$; (e) $E^z(x, y, t = 1.0)$; and (f) $E^z(x, 0, t = 1.0)$. The mesh size is 100×100.

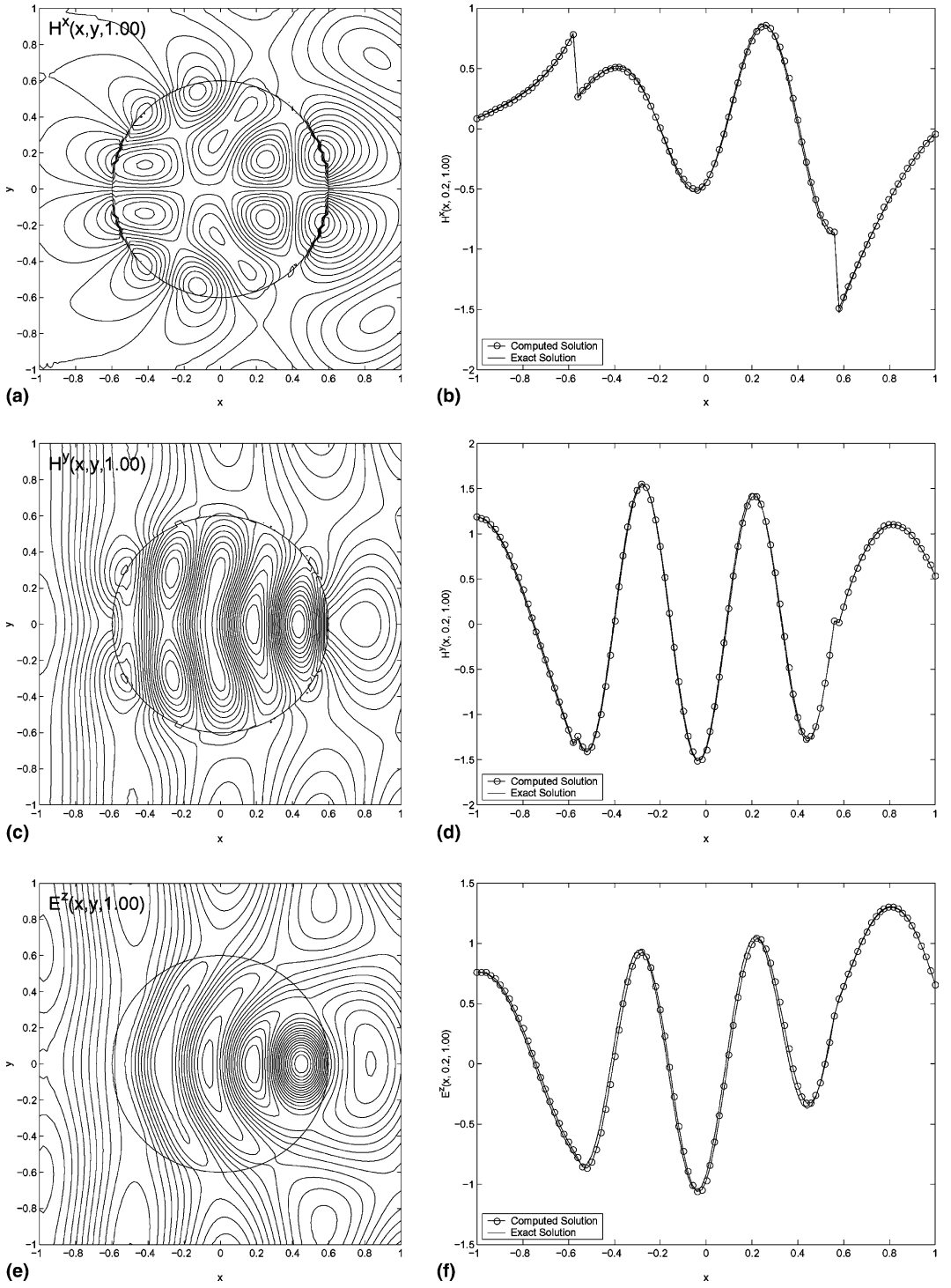

Fig. 10. Scattering of a 2D dielectric cylinder with material parameters $\mu_1 = \epsilon_1 = 1, \mu_2 = 2$ and $\epsilon_2 = 2.25$. On the left are contours of the computed solutions, and on the right are slices of the computed and the exact solutions. (a) $H^x(x, y, t = 1.0)$; (b) $H^x(x, 0.2, t = 1.0)$; (c) $H^y(x, y, t = 1.0)$; (d) $H^y(x, 0.2, t = 1.0)$; (e) $E^z(x, y, t = 1.0)$; and (f) $E^z(x, 0.2, t = 1.0)$. The mesh size is 100×100.

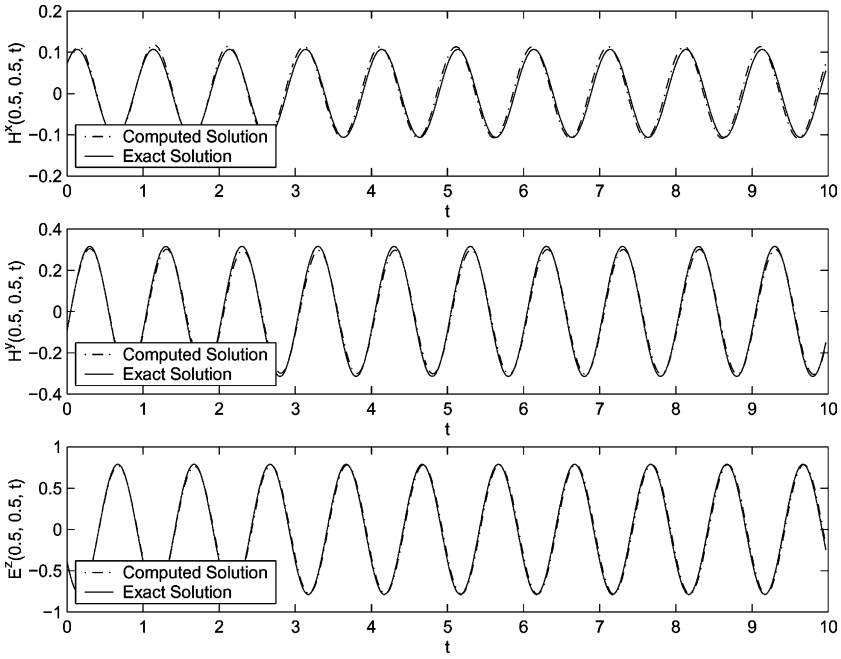

Fig. 11. Scattering of a 2D dielectric cylinder with material parameters $\mu_1 = \mu_2 = \epsilon_1 = 1$ and $\epsilon_2 = 2.25$. The plots are the computed and the exact time history of H^x, H^y and E^z at the point (0.5, 0.5). The mesh size is 100×100.

Figs. 9 and 10 show the contours and slices of the three computed field components at the time $t = 1.0$ for the first case ($\mu_2 = 1$) and the second case ($\mu_2 = 2$), respectively. Fig. 11 shows the time history of three field components at a fixed point $(0.5, 0.5)$ for the first case. Table 9 shows the grid refinement results for both cases, which again confirms the global second order accuracy.

Table 9
The grid refinement analysis for scattering of a 2D dielectric cylinder ($\epsilon_1 = 1,\ \epsilon_2 = 2.25,\ \mu_1 = 1,\ \mu_2 = 1$ or $\mu_2 = 2$)

$N \times M$	$\mu_2 = 1$		$\mu_2 = 2$	
	$\|E_N\|_\infty$	Order	$\|E_N\|_\infty$	Order
50×50	3.598×10^{-1}		6.988×10^{-1}	
100×100	7.059×10^{-2}	2.3498	1.648×10^{-1}	2.0840
200×200	1.696×10^{-2}	2.0569	3.454×10^{-2}	2.2544
400×400	4.179×10^{-3}	2.0212	7.933×10^{-3}	2.1225

Table 10
Comparison between the Yee's scheme and the UEBM for 2D Maxwell's equations – homogeneous medium ($\epsilon = 2.25$ and $\mu = 2$)

$N \times M$	Yee's scheme		UEBM	
	$\|E_N\|_\infty$	Order	$\|E_N\|_\infty$	Order
50×50	1.113×10^{-1}		3.292×10^{-1}	
100×100	2.908×10^{-2}	1.9364	8.905×10^{-2}	1.8863
200×200	7.258×10^{-3}	2.0024	2.300×10^{-2}	1.9530
400×400	1.827×10^{-3}	1.9901	5.872×10^{-3}	1.9697

Table 11
Comparison between the Yee's scheme and the UEBM for 2D Maxwell's equations – inhomogeneous media ($\epsilon_1 = \mu_1 = \mu_2 = 1$ and $\epsilon_2 = 2.25$)

$N \times M$	Yee's scheme		UEBM	
	$\|E_N\|_\infty$	Order	$\|E_N\|_\infty$	Order
50×50	1.191×10^{-1}		3.598×10^{-1}	
100×100	6.182×10^{-2}	0.9460	7.059×10^{-2}	2.3498
200×200	3.287×10^{-2}	0.9559	1.696×10^{-2}	2.0569
400×400	1.698×10^{-2}	0.9529	4.179×10^{-3}	2.0212

To compare the Yee's scheme and the UEBM for 2D Maxwell's equations, we first solve the equations in a homogeneous medium with $\epsilon = 2.25$ and $\mu = 2$. The errors of both approaches are showed in Table 10. We then consider the scattering of the above 2D dielectric cylinder with $\epsilon_1 = \mu_1 = \mu_2 = 1$ and $\epsilon_2 = 2.25$. As shown in Table 11, the global accuracy of the Yee's scheme is reduced to first order because it cannot model the interface correctly. And again, for an accuracy around 1%, the UEBM ends up superior.

6. Conclusion

The proposed upwinding embedded boundary method (UEBM) retains the simplicity of the Cartesian grid based method while providing uniform accuracy across material interfaces at a time step allowed on the uniform Cartesian mesh. Extensive numerical tests confirm the stability, global second order accuracy and ease of implementation of the method. Compared with the Yee's scheme based on the staggered grid, the method proposed has more unknowns as the later only has tangential components defined on a staggered grid. However, the method proposed here can be easily extended to 3D, which will be the subject of future work.

Acknowledgements

The authors thank the support of the AFOSR and the National Science Foundation (Grant Nos. CCR-9972251, CCR-9988375, CCR-0098140 and CCR-0098275) for the work reported in this paper. Thanks also are extended to Professor Jan Hesthaven for his assistance during the process of this work and Professor Qinghuo Liu for many useful discussions.

Appendix A. GKS stability analysis of (2.11) and (2.15)

The schemes (2.3) and (2.6) consist of two distinct one-sided difference formulae – one at $x_j < x_d$ and the other at the outflow boundary x_d (based on a nonuniform grid) for $x \leqslant x_d$. The GKS theory [20,21] was not applicable to the combined schemes (2.3) and (2.6) for $x \leqslant x_d$.

In the following, we will analyze the stability of the scheme in (2.11) or (2.15) using the GKS theory for the model wave equation (2.1) with $a > 0$ and $x_d \leqslant x < \infty$. Let us assume that the discontinuity is located at $x_d = -\beta\Delta x,\ 0 < \beta \leqslant 1$, the solution u_+^n is provided through the jump condition (2.10), and the solution at $x_0 = 0$ is given by either (2.11) or (2.15).

Approach I – upwinding.

$$u_0^{n+1} = u_0^n - \lambda(c_0 u_+^{n+1} + c_1 u_+^n + c_2 u_1^n) + \frac{\lambda^2}{2}(d_0 u_+^{n+1} + d_1 u_+^n + d_2 u_1^n), \tag{A.1}$$

where $c_i,\ d_i,\ i = 0, 1, 2$ are given in (2.14), and $\lambda = a\Delta t/\Delta x$. For GKS stability analysis, we consider a homogeneous boundary condition at x_d by setting $u_+^n = u_+^{n+1} = 0$. Then we have

$$u_0^{n+1} = u_0^n + \left(\frac{\lambda^2}{2} d_2 - \lambda c_2\right) u_1^n. \tag{A.2}$$

Approach II – interpolation.

$$u_0^{n+1} = e_0 u_+^{n+1} + e_2 u_1^{n+1} + e_3 u_2^{n+1}, \tag{A.3}$$

where $e_0,\ e_2,\ e_3$ are given in (2.16). Again for GKS stability analysis, we can set $u_+^{n+1} = 0$. We have

$$u_0^{n+1} = e_2 u_1^{n+1} + e_3 u_2^{n+1}. \tag{A.4}$$

For $j \geqslant 1$, we have the regular Lax–Wendroff scheme

$$u_j^{n+1} = \frac{\lambda(1+\lambda)}{2} u_{j-1}^n + (1-\lambda^2) u_j^n - \frac{\lambda(1-\lambda)}{2} u_{j+1}^n. \tag{A.5}$$

For GKS stability analysis, we need to show that the scheme (A.2) and (A.5), or (A.4) and (A.5) does not have any nontrivial admissible solution of the following form

$$u_j^n = A(z) z^n \kappa^j, \qquad |z| \geqslant 1, \quad |\kappa| \leqslant 1. \tag{A.6}$$

For the scheme (A.2) and (A.5), we have the following system

$$\begin{cases} z = 1 + \left(\frac{\lambda^2}{2} d_2 - \lambda c_2\right)\kappa, \\ z = \frac{\lambda(1+\lambda)}{2}\kappa^{-1} + (1-\lambda^2) - \frac{\lambda(1-\lambda)}{2}\kappa. \end{cases} \tag{A.7}$$

Then it can be checked numerically that for $0 \leqslant \lambda < 1$ and $0 < \beta \leqslant 1$, the system (A.7) has no admissible solutions which satisfy $|z| \geqslant 1$ and $|\kappa| \leqslant 1$.

Similarly, for the scheme (A.4) and (A.5), we have

$$\begin{cases} 1 - e_2\kappa - e_3\kappa^2 = 0, \\ z = \frac{\lambda(1+\lambda)}{2}\kappa^{-1} + (1-\lambda^2) - \frac{\lambda(1-\lambda)}{2}\kappa. \end{cases} \tag{A.8}$$

From the first equation, we can see that

$$\kappa = \frac{\beta+2}{\beta+1} \pm \frac{\sqrt{\beta+2}}{\sqrt{\beta}(\beta+1)}\sqrt{-1},$$

which is shown to be greater than 1 in magnitude for $0 < \beta \leqslant 1$. Thus, the system (A.8) has no admissible solutions either.

Together this proves the stability of (2.11) and (2.15).

References

[1] A. Taflove, Computational Electrodynamics – The Finite Difference Time-Domain Method, Artech House, Boston, 1995.
[2] R.F. Harrington, Field Computation by Moment Methods, Macmillian, New York, 1968.
[3] K.S. Yee, Numerical solution of initial boundary value problems involving Maxwell equations in isotropic media, IEEE Trans. Antenn. Propag. 14 (1966) 302.
[4] A. Ditkowski, K. Dridi, J.S. Hesthaven, Convergent Cartesian grid methods for Maxwell's equations in complex geometries, J. Comput. Phys. 170 (2001) 39.

[5] B. Cockburn, C.W. Shu, The local discontinuous Galerkin finite element method for convection-diffusion systems, SIAM J. Numer. Anal. 35 (1998) 2440.
[6] P. LeSaint, P.A. Raviart, On a finite element method for solving the neutron transport equation, in: C. De Boor (Ed.), Mathematical Aspects of Finite Elements in Partial Differential Equations, Academic Press, New York, 1974, p. 89.
[7] D. Kopriva, S.L. Woodruff, M.Y. Hussaini, Discontinuous spectral element approximation of Maxwell's equations, in: B. Cockburn, G. Karniadakis, C.-W. Shu (Eds.), Discontinuous Galerkin Methods: Theory, Computation and Applications, Springer, New York, 2000, p. 355.
[8] T. Warburton, Application of the discontinuous Galerkin method to Maxwell's equations using unstructured polymorphic hp-finite elements, in: B. Cockburn, G. Karniadakis, C.-W. Shu (Eds.), Discontinuous Galerkin Methods: Theory, Computation and Applications, Springer, New York, 2000, p. 451.
[9] M.J. Berger, R.J. LeVeque, Adaptive Cartesian mesh algorithm for the Euler equations in arbitrary geometries, AIAA paper 89-1930, June, 1989.
[10] H. Forrer, M.J. Berger, Flow simulations on Cartesian grid involving complex moving geometries, in: Proceedings of the International Conference on Hyperbolic Problems, Zurich, Switzerland, February, 1998.
[11] R.J. LeVeque, Z. Li, The immersed interface method for elliptic equations with discontinuous coefficients and singular sources, SIAM J. Numer. Anal. 31 (1994) 1019.
[12] C. Zhang, R.J. LeVeque, The immersed interface method for acoustic wave equations with discontinuous coefficients, Wave Motion 25 (1997) 237.
[13] R.E. Collin, Field Theory of Guided Waves, IEEE Press, New York, 1991.
[14] Z. Zhang, Ultraconvergence of the patched recovery technique II, Math. Comp. 69 (2000) 141.
[15] J.P. Berenger, A perfectly matched layer for the absorption of electromagnetic waves, J. Comput. Phys. 114 (1994) 185.
[16] R. Ziolkowski, Time derivative Lorentz model based absorbing boundary condition, IEEE Trans. Antenn. Propag. 45 (1997) 1530.
[17] S. Abarbanel, D. Gottlieb, On the construction and analysis of absorbing layers in CEM, Appl. Numer. Math. 27 (1998) 331.
[18] P. Lorrain, D. Corson, F. Lorrain, Electromagnetics Fields and Waves, W.H. Freeman and Company, New York, 1988.
[19] K. Umashankar, A. Taflove, Computational Electrodynamics, Artech House, Boston, 1993.
[20] B. Gustafsson, H.O. Kreiss, A. Sundstrom, Stability theory of difference approximations for mixed initial boundary value problems II, Math. Comput. 26 (1972) 649.
[21] J. Strikewerda, Finite Difference Schemes and Partial Differential Equations, Wadsworth and Brooks/Cole, 1989.